Available online at www.sciencedirect.com
ScienceDirect
Ultramicroscopy 106 (2006) 1024–1032
ultramicroscopy
www.elsevier.com/locate/ultramic

Mapping chemical and bonding information using multivariate analysis of electron energy-loss spectrum images

M. Bosman[a,*], M. Watanabe[b], D.T.L. Alexander[c], V.J. Keast[a]

[a]*Australian Key Centre for Microscopy and Microanalysis, University of Sydney, Sydney, NSW 2006, Australia*
[b]*Department of Materials Science and Engineering, Lehigh University, Bethlehem, PA 18015, USA*
[c]*Department of Materials Science and Metallurgy, University of Cambridge, Pembroke St. CB2 3QZ, UK*

Received 23 June 2005; received in revised form 26 October 2005; accepted 18 April 2006

Abstract

Electron energy-loss spectroscopy (EELS) in the transmission electron microscope (TEM) is used to obtain high-resolution information on the composition and the type of chemical bonding of materials. Spectrum imaging, where a full EEL spectrum is acquired and stored at each pixel in the image, gives an exact correlation of spatial and spectral features. However, determining and extracting the important spectral components from the large amount of information contained in a spectrum image (SI) can be difficult. This paper demonstrates that principal component analysis of EEL SIs can be used to extract chemically relevant components. With weighted or two-way scaled principal component analysis, both compositional and bonding information can be extracted. Mapping of the chemical variations in a partially reduced titanium dioxide sample and the orientation-dependent bonding in boron nitride and carbon nanotubes are given as examples.

PACS: 02.50.Sk; 79.20.Uv

Keywords: Principal component analysis; EELS; Spectrum imaging

1. Introduction

Transmission electron microscopy (TEM) is widely used to study the structure of materials at high spatial resolution. This structural information is often complemented by compositional information obtained with integrated spectroscopic techniques such as X-ray energy-dispersive spectroscopy (XEDS) and electron energy-loss spectroscopy (EELS). In the latter technique, the energy of the inelastically scattered electron beam is measured as it passes through a thin TEM specimen. It is common to divide the EEL spectrum into two regions, the low-loss region below about 50 eV and the core-loss region beyond this value. In the low-loss region, information on interband transitions and plasmon excitations can be found. The core-loss EEL spectrum contains ionisation edges, resulting from atomic core electrons that have been excited to unoccupied states. The unoccupied density of states (DOS) and, therefore, the shape of the ionisation edge will vary with changing bonding environments. This may, for example, be due to the local presence of different chemical elements, mechanical strain, variation in ionic valency, and so on [1]. The changes in the EEL spectra due to changes in bonding environment are rather subtle, and give rise to mostly small modulations of the ionisation edges, called the energy-loss near-edge structure (ELNES) [2]. The ability to obtain high-resolution information on the type of bonding [3–6], as well as the chemical composition, has given rise to the widespread use of EELS in materials science.

EEL spectra with high spatial resolution can be obtained by using a small-diameter electron probe in a scanning TEM (STEM) and placing it on the feature of interest. However, in recent years, the focus of analytical electron microscopy has moved away from single spectrum acquisition to mapping and imaging. This is performed

*Corresponding author.
E-mail address: michel.bosman@emu.usyd.edu.au.au (M. Bosman).

0304-3991/$ - see front matter © 2006 Elsevier B.V. All rights reserved.
doi:10.1016/j.ultramic.2006.04.016

by scanning the focused electron beam in a raster of pixels, while, at each pixel, an EEL spectrum is acquired. In this way, a three-dimensional data cube with two spatial axes and one energy axis is obtained. This data cube is called an EEL spectrum image (SI) and allows the precise correlation between spatial and spectral features [7,8]. However, extracting the small modulations of the plasmon peaks or ionisation edges is not always straightforward and may demand sophisticated analysis of the spectra. Whilst routines such as multiple least-squares fitting of reference spectra or curves can be used, they require prior knowledge from the operator as to what spectral features are expected. In a SI, which may contain many thousands of spectra and where all the possible spectral components are not known, there is a clear need for (semi-) automatic data processing procedures.

Multivariate statistical analysis (MSA) [9] is a useful family of technique to analyse large datasets, which contain many known and/or unknown variables. It has been used in a wide range of research fields, for example, geological remote sensing [10], X-ray absorption spectroscopy [11], scanning probe microscopy [12], and electron microscopy [13–16], to gain insight into spectral data. Principal component analysis (PCA) is one of the most popular MSA approaches and is also widely performed as a first step to other, more advanced MSA approaches. The general concept of PCA is to reduce the dimensionality of an original large dataset by finding a minimum number of variables that describe the original dataset without losing any significant information [17]. Without any prior knowledge of the dataset, PCA extracts the variables as mutually independent "abstract components". A more detailed description of PCA is given in the next section.

Since the first application to EELS by Trebbia and Bonnet [13], PCA has been applied to segregation studies measured by XEDS, and EELS line-scans [14–16,18]. In this work we will demonstrate that PCA can be extended to EEL SIs, as opposed to line scans and, in particular, can be used to extract and *map* the bonding components. It will also be shown that EELS SIs have their own distinct challenges for PCA analysis as compared to other data sets, and possible routines to deal with these particularities are given. We have applied this approach to three materials systems. In the first case, a sample of mixed titanium oxides and calcium titanate has been analysed using a low-loss EELS SI. In the second and third examples, the ELNES of core-loss SIs has been studied to map the orientation of the chemical bonding of boron nitride and carbon nanotubes, respectively.

2. Theoretical background

To decompose an EEL SI, it first needs to be described as a two-dimensional data matrix $\mathbf{D}_{((x,y),E)}$. This is done by combining the two spatial dimensions (x, y) and storing them in the columns of the data matrix, while the spectral information (E) is stored in the rows. By applying PCA, this data matrix can be decomposed as [9]

$$\mathbf{D}_{((x,y),E)} = \mathbf{S}_{((x,y),n)} \times \mathbf{L}^{\mathrm{T}}_{(E,n)}, \tag{1}$$

where $\mathbf{S}_{((x,y),n)}$ is called the score matrix and $\mathbf{L}_{(E,n)}$ the loading matrix; the superscript T of $\mathbf{L}$ represents a matrix transpose. When describing a SI dataset, each row of $\mathbf{L}^{\mathrm{T}}$ contains a spectral feature uncorrelated to the other rows and can be called an eigenspectrum of the dataset. On the other hand, each column of $\mathbf{S}$ represents the spatial amplitude of the corresponding eigenspectrum in the loading matrix. The individual product of each row of the loading and column of the score matrices is called a principal component. The number of principal components is n and will be mathematically equal to the smaller number of $x \cdot y$ or E.

In practice, the matrix decomposition can be performed by applying eigenanalysis or singular value decomposition to the data matrix [9,17], with the singular values being equivalent to the square root of the eigenvalues. The relative magnitude of each eigenvalue indicates the amount of variance that the corresponding principal component contributes to the dataset. In the decomposed matrices, the principal components are ordered from high to low, according to their eigenvalues and so is the variance—or information that they describe.

Typically, the number of dominant features in the dataset is much less than n, and the last principal components will therefore describe experimental noise. If the number of non-noise principal components is determined, the original dataset can be reconstructed using this limited number of principal components, α:

$$\tilde{\mathbf{D}}_{((x,y),E)} = \mathbf{S}_{((x,y),\alpha)} \times \mathbf{L}^{\mathrm{T}}_{(E,\alpha)}. \tag{2}$$

Here, $\tilde{\mathbf{D}}$ is the reconstructed data matrix calculated using a linear combination of the first α principal components, where $\alpha \ll n$. As a result of the reconstruction, the experimental noise can be removed efficiently from the original dataset without sacrificing spatial or energy resolution.

Many methods have been developed to determine α, the number of information-carrying principal components [19]. Unfortunately, there is no universal rule of thumb, but one of the most common approaches is to plot the logarithms of the eigenvalues versus the component number, in a so-called "scree plot". Since the eigenvalues of subsequent, random noise-containing principal components decrease exponentially, the components that only describe experimental noise should lie on a straight line in the scree plot; an example will be given in the Section 4. In summary, PCA is a technique to

(1) identify independent spectral features as abstract principal components, and
(2) reduce random noise components efficiently in a statistical manner.

Before doing PCA, additional mathematical preprocessing of the datasets can be useful to minimise mixing of the various spectral features in the loading spectra. The most common preprocessing routines are centering (subtracting the average values or constant values from the dataset) and scaling (dividing the data set by a constant value or a weighted average, also called weighting), and these can be applied to one of the data matrix directions (spatially or spectrally) or both directions [20]. The effectiveness of such preprocessing for PCA again depends very much on the type of dataset. Keenan and Kotula discussed efficient preprocessing for time-of-flight secondary ion mass spectrometry (ToF-SIMS) SI datasets [21]. They concluded that the best preprocessing is two-way scaling or weighting, based on Poisson counting statistics. The justification of this method is that the experimental noise varies with detector channel and pixel number; e.g. the experimental noise in a minor spectral feature is less than in the energy channels of a peak with high intensity. Weighting will reorganise the data in order to normalise the distribution of the experimental noise. In this study, PCA was performed without and with prior weighting, as implemented with the data transformation method proposed by Cochran and Horne [22].

3. Experimental

In section 4.1, results will be presented of the analysis on partially reduced titanium dioxide. A powder-pressed TiO_2 cathode was electrochemically reduced in molten $CaCl_2$, in a new technique to extract pure titanium from its ore [23]. A TEM sample from the cross-section of the partially reduced TiO_2 has been prepared using standard tripod polishing routines and ion milling to electron transparency. A low-loss EEL SI has been taken from this sample, and PCA is performed. Although the loading spectra from the complex low-loss part of the spectrum may not be readily interpretable as will be discussed later, the score images will prove to be helpful in extracting chemical information from this technologically valuable sample.

The second example will present weighted PCA on a core-loss EEL SI of a standard specimen of boron nitride flakes on an amorphous carbon support grid. The ionisation edges for this material have been studied thoroughly and are well understood. Another example of weighted PCA to extract ELNES features is given in the third example. Here, the core-loss SI of a carbon nanotube is obtained, and the spectral components are analysed and mapped. To prepare this sample, commercially available multiwall carbon nanotubes (Sigma-Aldrich) were dispersed in ethanol and deposited on an amorphous carbon support grid.

The measurements of the reduced titanium oxide and boron nitride specimen were performed using a JEOL 3000F TEM, operated in scanning mode at an acceleration voltage of 300 kV. This microscope is equipped with a Schottky field-emission gun (FEG) and a Gatan image filter (GIF) to acquire the energy loss spectra. To optimise the signal-to-noise ratio for each spectrum, a 150 μm condenser lens aperture, 0.7 nm electron beam spot size and 15 cm camera length settings were used. To further improve the electron flux to the detector, a large spectrometer entrance aperture of 3 mm was used. The energy resolution obtainable with these settings is 1.5 eV full-width at half-maximum (FWHM) of the zero-loss peak, which was sufficient to resolve the spectral features of interest in these examples.

Reference spectra of standard samples of different titanium oxides (i.e., anatase TiO_2, Ti_5O_9, Ti_4O_7, Ti_2O_3 and TiO) were acquired using a VG 601UX dedicated STEM with a cold FEG and equipped with a Gatan 677 parallel EELS detection system, operating at 100 kV. By defocusing the electron beam, the current density was sufficiently lowered to avoid radiation damage—in particular reduction under the electron beam—while taking a measurement. Note that when such damage did occur, it had an obvious effect on the EEL spectrum. The same microscope, now equipped with a Gatan Enfina EELS detector, has been used for acquiring SIs of the carbon nanotube. Using a spectrometer entrance aperture of 4 mm, this system had an energy resolution of 0.6 eV with the 677 parallel EELS and 0.4 eV with the Enfina, under similar conditions.

Spectrum imaging was controlled by Digital Micrograph software, version 3.9.0 by Gatan Inc. Typical integration times of 0.3–1 s per spectrum were used, giving an acquisition time in the order of 20 min for a whole SI. During acquisition, dark current and detector gain variations were automatically removed from the spectra, and spatial drift was corrected.

Spectra in raw, unprocessed SIs may contain similar artefacts as single EEL spectra and need to be processed in the conventional way. Additionally, in a SI, the energy axes of the spectra may be misaligned due to energy drift during acquisition and this should be corrected. Using the post-acquisition routines available in Digital Micrograph, X-ray spikes were removed from the spectra, followed by alignment of the mutual energy scales of the spectra. This was done by fitting a Gaussian curve to a sharp feature in the spectrum, and using the energy position of this curve in every spectrum to correct for any misalignments.

Only spectral features that arise from single scattering events are useful for interpretation. To remove plural scattering from the spectra, Fourier-log deconvolution [1] is used on the low-loss EEL SI, while Fourier-ratio deconvolution has been performed on the boron nitride core-loss SI using the accompanying low-loss SI. The carbon nanotube in the third sample was sufficiently thin that plural scattering could be disregarded, and no deconvolution was necessary. Fourier deconvolution can introduce higher-order oscillation artefacts in typically one in a few 100 spectra, and the spectrum in these pixels was then replaced by the average of its surrounding spectra [24]. For the core-loss SIs, the spectral background signal was

extrapolated and removed from every spectrum using the power law routine. The ZLP was removed from the low-loss spectra of the reduced oxide sample using the reflected tail model. In this, a reflection of the left-side tail of the ZLP is used to model the tail on the energy-loss side. The final processing step is to trim the spectra so that they only contain the energy range of interest.

PCA is performed using a computer program that has been developed in C++ language by incorporating the CLAPACK routine [25]. To perform the matrix decomposition of large SI datasets efficiently, the basic linear algebra parts of CLAPACK have been optimised to AMD central processing units by employing the automatically tuned linear algebra software (ATLAS) package [26]. This program includes an option for weighting the data prior to PCA, using a data transformation method.

Since the data have not been centred around a mean value, the first loading spectrum always resembles the average of all measured spectra. The loading spectra of higher-order principal components have a mean value of zero, and will therefore contain both positive and negative intensities, depending on how much the spectral feature they represent deviates from this average spectrum. Interpretation of loading spectra will, therefore, not be completely straightforward since they do not contain real EEL spectra. A certain degree of insight in the interpretation of component spectra is required, as will be shown in the following examples.

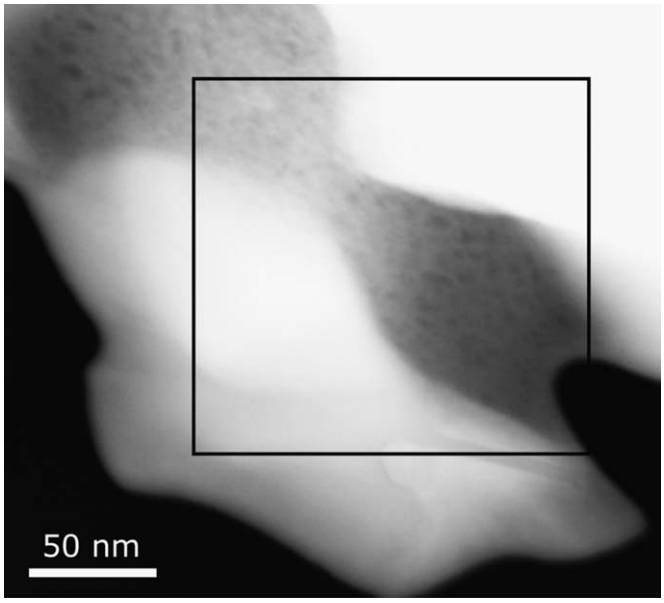

Fig. 1. ADF image of a thin section of the reduced titanium oxide sample. The black square indicates the region where the SI was acquired.

4. Results

4.1. Identification of phases in calcium-containing titanium oxide

Fig. 1 shows a high-angle annular dark field (HAADF) image of a specimen taken from a cross-section of the reduced oxide cathode material, which was found to contain a calcium-titanate phase as well as various titanium oxides. The black spots in the central vertical section may be thickness variations or defects caused by ion milling. The black square indicates the area from which the low-loss EEL SI was taken. The trimmed SI had dimension of 60×56 pixels by 621 energy channels. The Fourier-log deconvolution removed multiple scattering effects, as well as the zero-loss peak, while the energy range covered 3.0–65.1 eV. After acquisition and preprocessing, as described above, PCA was performed.

Fig. 2 displays the score images of the first six principal components. The 7–621st principal components contain only noise, thus the first six components represent all the relevant spectral information. The light-coloured pixels of the score images represent areas of the sample where the corresponding loading spectrum is defined most strongly. As mentioned in the previous section, the first score image corresponds to the average spectrum, so no individual phase information can be interpreted from it. On the other

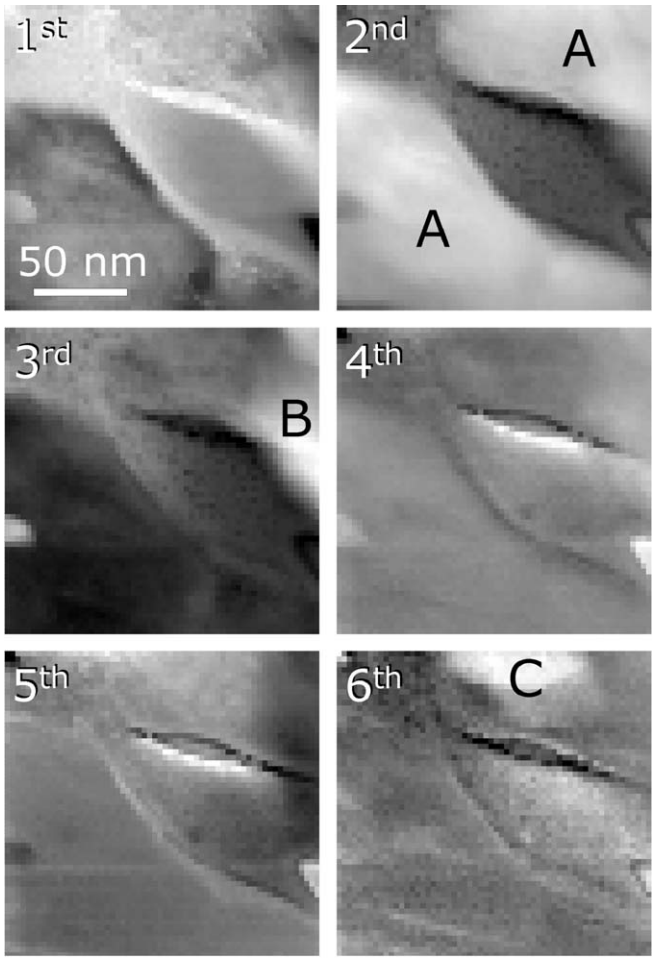

Fig. 2. Score images of the first 6 principal components of the low-loss SI, taken from the area indicated in Fig. 1.

hand, the next five principal components all carry compositional and phase information.

The score images show some regions of interest, labelled A–C. The second score image looks very similar to the HAADF, and may therefore wrongly be interpreted as containing thickness information. However, since the spectra have been Fourier-log deconvolved, none of the score images contain direct information on the sample thickness; only the HAADF does. Going back to the SI and summing the spectra from these regions of interest reveals what chemical information is carried in each principal component. The summation of spectra from these regions is displayed in Fig. 3.

All three spectra display an easily recognisable feature at 47.5 eV. This is the titanium $M_{2,3}$ edge, representing transitions from electrons in the titanium $3p_{1/2}$ and $3p_{3/2}$ core shells to empty energy states in the conduction band. The third score image in Fig. 2 shows two bright regions on the left and right-hand side, indicated area B. The summed spectra in these pictures, given in Fig. 3, show a strong feature around 35 eV energy loss, which arises from the calcium $M_{2,3}$ edge. The white regions, labelled B in the third score image, therefore show areas that are rich in calcium, i.e. calcium titanate. These areas are not distinctly present in the HAADF since the density of anatase titanium dioxide (4.2 g/cm^3) is very similar to the density of calcium titanate (4.1 g/cm^3). This difference is so small that it will not cause a notable difference in the elastic scattering intensity as detected by the HAADF. Thus the bright areas in the HAADF image are mostly caused by thickness variations, not local changes in density.

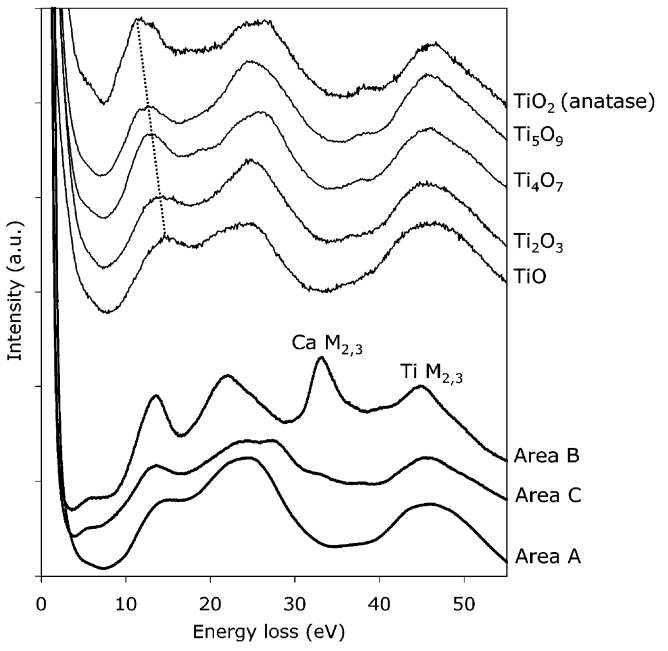

Fig. 3. Summed EEL spectra from areas A–C as indicated on the score images of Fig. 2. A series of EEL spectra from standard titanium oxide samples with varying oxidation state is displayed as thin lines. The dotted line indicates the systematic change of the 12–15 eV spectral feature.

The light pixels in score images four and five contain carbon plasmon spectra, indicating areas where organic molecules have deposited during acquisition or during sample preparation. The score image of the sixth principal component images the presence of another source of variation, indicated by area C in Fig. 2. The summed spectra of this region are displayed in Fig. 3, and show a slight difference compared to the summed spectra from region A, mainly around 25–28 eV energy loss. To gain more insight into this small spectral difference, EEL spectra collected from standard titanium oxide samples of known chemical composition are displayed in Fig. 3. It is known that the spectral feature between 12 and 15 eV energy loss characterizes the arrangement of the TiO_6 octahedra [27], and systematically changes with varying oxidation state. Together with the peak position of the 25–28 eV feature, it can be used to qualitatively identify the phases of the different regions. This analysis shows that area A mainly constitutes TiO, while area C in the sixth score image consists of a mixture of Ti_2O_3 and a less reduced titanium oxide, possibly Ti_4O_7 or TiO_2; additionally, small amounts of calcium might be present. Since the spectra of areas A and C differ only slightly, manually scanning over the SI and observation initially did not reveal the presence of the latter phase. PCA however, clearly extracted its presence. This complex mix of different oxides on a relatively fine scale had not been expected and may be relevant to the development of this processing route for titianium dioxide reduction.

4.2. Extracting ELNES features from a BN sample

An ADF image of the boron nitride specimen is shown in Fig. 4. The white rectangle indicates the area from which the SI was taken. The SI had dimension of 49×25 pixels and covered an energy range of 180.1–440.2 eV with a dispersion of 0.3 eV per channel. PCA with and without prior weighting has been performed on the SI. Fig. 5 shows the scree plot for both methods. Principal components that only contain experimental noise can be identified in the

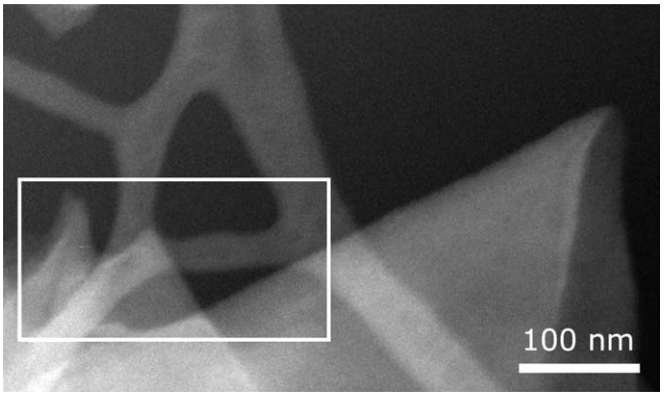

Fig. 4. Annular dark field image of the boron nitride flakes on an amorphous carbon support grid. The white square indicates the region where the SI is taken.

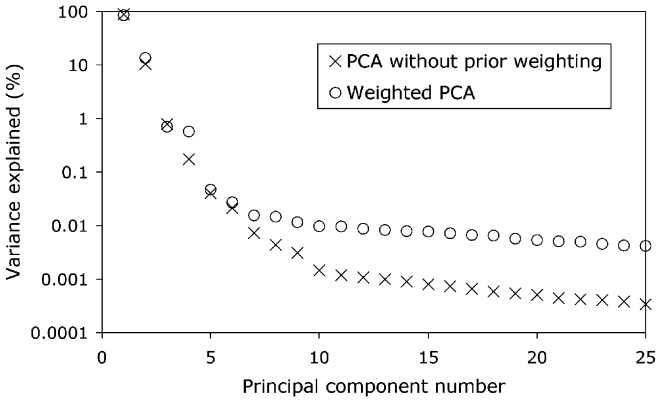

Fig. 5. The information captured in the first 25 principal components of the BN sample. The higher components that lie on a straight line represent noise. For PCA without prior weighting, as well as for weighted PCA, the first component explains about 85% of the variance in the data.

linear part of this logarithmic plot. The curve resulting from PCA without prior weighting shows nine non-noise components diverging from this straight line. Weighted PCA on the same SI results in just six non-noise components. The chemical information is thus captured in fewer components, leading to better interpretability [16].

Score images and loading spectra resulting from weighted PCA are given in Fig. 6. The first component, again, gives the average spectrum and its loading in each pixel. Three main features can be seen in the spectrum, the boron-K ionisation edge, the carbon-K edge, and the nitrogen-K edge, all resulting from electron transitions from the atomic 1s orbital of that element to the conduction band. The second principal component shows the anticorrelation between the BN and the carbon; in the score image, carbon is light and BN is dark.

The third principal component identifies a systematic artefact due to incorrect background subtraction. As usual, a power-law fit to the boron pre-edge was subtracted from each spectrum. In this case, however, the model did not perfectly fit the background signal, a result that was reproducible with other data sets taken from BN with a different microscope. Therefore, with the somewhat misfitting power-law model, the background-subtracted spectra will show a slightly upwards-sloping signal where they should be flat. This false signal becomes particularly distinct beyond 350 eV, far from the background-fitting window. This upwards-sloping curve will be the only 'signal' present in spectra that were taken off the specimen, which explains why the third principal component is well defined in these pixels. Only spectra taken from carbon-rich regions will show an overall *downwards*-sloping curve beyond 350 eV; boron nitride on the other hand will have a relatively high signal after 350 eV due to the nitrogen K-edge. This explains why the upwards slope of the third principal component is strongly anti-correlated with the carbon-K-edge, but hardly with the BN edges.

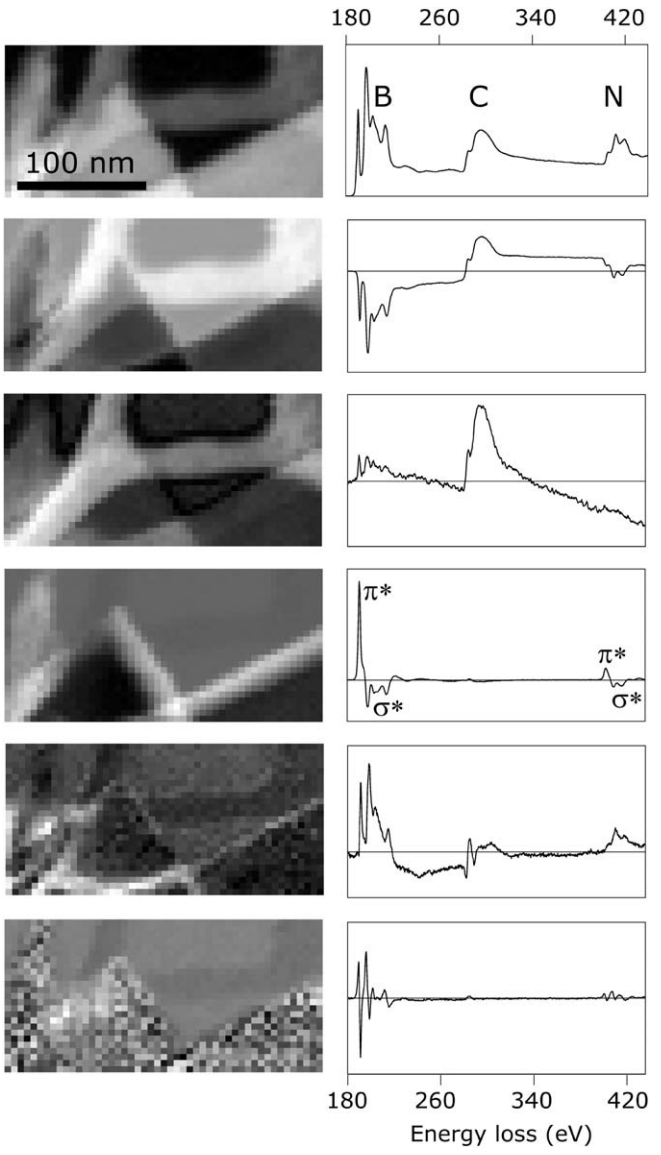

Fig. 6. Score images and loading spectra of the first 6 principal components of the BN sample shown in Fig. 4, extracted using weighted PCA.

The fourth principal component is interesting in the sense that it contains information on the ELNES of the material. This component shows the anticorrelation between the π^* and σ^* features of both the boron and nitrogen ionisation edges. The π^* peak is related to the sp^2 bonds in this material, which are highly directional in nature. The intensity of the π^* peak can therefore be related to the orientation of the planar sheets relative to the electron beam. In the experimental conditions used here the momentum transfer is primarily perpendicular to the electron beam. So, the white areas in the fourth score image show where the electron beam is almost parallel to the BN sheet direction, while in the dark regions the sheets are perpendicular to the electron beam. Therefore, the fourth principal component contains orientation information, and the BN sheets appear to be curled up near the

edges. The next section will show similar results that confirm this explanation. The fifth principal component is the result of slight spatial misalignment between the low-loss SI and the core-loss SI during Fourier-ratio decomposition. This minor misalignment results in spectral artefacts in areas of strong thickness variation, as can be seen in the fifth score image. Finally, the sixth principal component results from a slight energy-scale misalignment of the spectra.

4.3. ELNES mapping of a carbon nanotube

Fig. 7 shows the loadings and score images of a core-loss SI taken from a multiwalled carbon nanotube. In addition to the first principal component, representing the average spectrum, only one other non-noise component was extracted using weighted PCA. This second principal component contains information on the chemical bonding. As with the boron nitride specimen, the ELNES of carbon nanotubes contains information on the orientation of the graphene sheets. The π^* peak is relatively higher at the edges of the nanotubes where the sheets are parallel to the electron beam than at the centre when they are perpendicular to the beam. The score image of the second principal component therefore maps the orientation of the chemical bonds.

A summation of all the spectra from the residual SI, reconstructed from the remaining 3rd and higher-order principal components, shows random noise. This indicates that all the chemically relevant information is carried by the first two weighted principal components; the other principal components have extracted the experimental noise. When the same SI is analysed using PCA without prior weighting, the first two principal components are in this case almost identical to the ones obtained with weighted PCA.

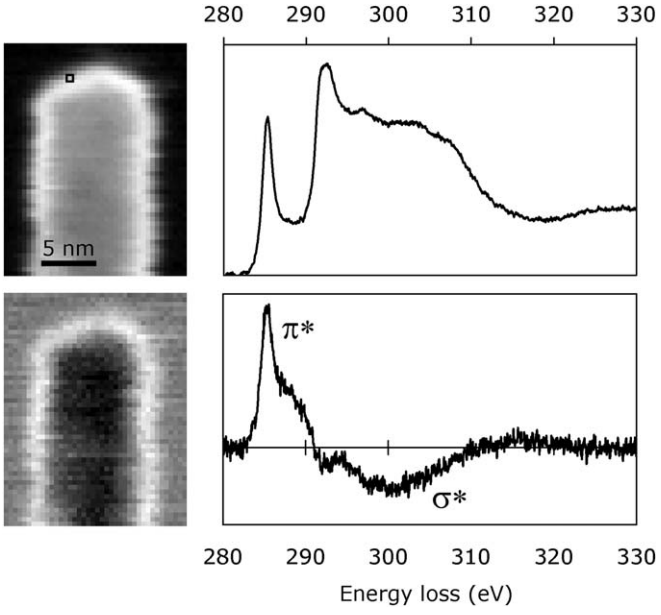

Fig. 7. First two score images and loading spectra from the multiwalled carbon nanotube sample, as extracted by weighted PCA. The black square in the first score image indicates the pixel from which the spectra of Fig. 8 were taken.

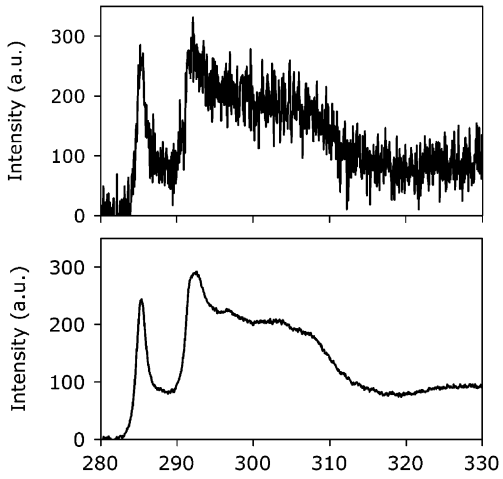

Fig. 8. Top: the spectrum from one pixel in the original SI, before principal component analysis. Bottom: the spectrum from the same pixel (as indicated by the black square in the first score image of Fig. 7), taken from the reconstructed SI. Reconstruction was done using the first two weighted principal components, also displayed in Fig. 7.

Fig. 8 shows the spectrum in a pixel from both the original and reconstructed SI. The original spectra in all pixels are very noisy, even more so in this pixel since it is taken at the edge of the nanotube, as indicated in Fig. 7. After the SI has been reconstructed using the first two weighted principal components, the spectrum in this pixel has a remarkably better signal-to-noise ratio, indicating the usefulness of PCA in removing noise from the spectra. Additionally, unlike other noise-removing routines (e.g. smoothing), the energy resolution is not degraded. The reason for this advantage is that PCA is a multivariate technique, applying a statistical analysis to many spectra, while smoothing is a univariate technique, analysing each spectrum individually.

5. Discussion

This work has shown that PCA analysis of EELS SIs can extract both compositional and ELNES components and map them. In the examples of boron nitride and the carbon nanotubes the systems were already well understood and we have shown that PCA analysis produces the expected results with regard to the compositional and orientation information. On the other hand, in the example of the reduced titanium dioxide sample, it was shown that PCA can identify spectral features in the SI that may not be noticed or anticipated by the operator. This specimen had a complex oxide structure made up of several phases. In one small area of the region from which the SI was taken the PCA score images indicated that a separate phase with higher oxidation state was present. This separate phase had not been noticed in previous analysis of this SI. The other

most striking advantage of PCA is that reconstructing the SI using only the significant components, and neglecting all the noise components, provides a very reliable way of removing experimental noise from spectra and SI data sets. The effectiveness of PCA in this regard when compared with other techniques is a consequence of the fact that all data is processed as a whole, instead of as individual spectra.

An important difference of EELS with other spectrum imaging techniques like XEDS is that the energy position of the peaks in the spectrum is not necessarily fixed. This makes the SI with the reduced titanium dioxide fundamentally different from the other two data sets. As is the case in many low-loss EEL spectra, peaks will shift in energy going from one phase to another. This introduces extra dimensions to the data set, making it impossible to extract a shifting peak as one single component. The various loading spectra that contain this peak will be very difficult to interpret, and a different approach is preferred. One obvious way to extract a peak shift from a SI is to non-linearly fit a Gaussian to it, and extract the map of the central position of the Gaussian. More sophisticated non-linear approaches may be useful too, but are usually rather involved. However, instead of using PCA as an explanatory method, it may be used in an explorative manner. The PCA approach presented here, where the score images were just used to extract areas of interest, proved effective in extracting an unanticipated phase. For an explanatory analysis, PCA is most useful in situations were peaks and edges in the different spectra are not shifting in energy. The extracted score images can then be directly interpreted via the loading spectra, as was shown in the BN and carbon nanotube examples.

The ability of PCA to extract minor, but significant components, which is one of its main advantages, is also one of its main limitations. If even only one spectrum in the whole SI contains an artefact, this will appear as a component. Similarly, a very small intensity artefact, but which is present in a number of spectra, will also appear as a component. In this latter case, this component may become "mixed" with a real component of interest, such as was the case with the 3rd component in the boron nitride SIs, which is thought to be an artefact due to incorrect background signal subtraction. In the same data set, the sixth principal component is an artefact due to remaining energy misalignments. As explained in the experimental section, Gaussians are fitted to align the energy scales in all spectra. But unfortunately, a misalignment of one or two energy channels will always remain, for example when the maximum of the spectral feature used for alignment consists of two channels with the same intensity. This slight remaining misalignment is most notable for sharp spectral features, like the ones present in the boron *K*-edge in this case.

Artefacts like these in the spectra, which may not be significant when applying more conventional processing methods, make the interpretation of PCA results difficult. Therefore, the greatest of care must be taken in the acquisition and preprocessing of the EELS SIs. Experimental artefacts which must be addressed include: systematic errors in the gain and dark current collection, X-ray spikes, energy drift and multiple scattering deconvolution errors. Similarly, carbon contamination and beam damage can add extra components and make further analysis very difficult. However, as we have discovered in the course of these experiments, using PCA to process a SI dataset can be a very effective way to test how well the spectrometer and microscope are performing. Experimental artefacts that may not have been noticed in a simple examination of the spectra are readily revealed by the PCA. It may, for example, be used to test if deconvolution is needed, since the non-linear effect of multiple scattering will show up as extra components in thicker parts of the specimen.

When there are just a few, well-defined components, as in the case of the carbon nanotube sample, PCA without prior weighting may lead to results that are very similar to results obtained with weighted PCA. In contrast, the more complex sample of BN on amorphous carbon demonstrated the usefulness of weighted PCA; the same amount of information is then described in fewer components. In the case of weighted PCA, there is less mixing between the various chemical signals in the loading spectra, making the individual components easier to interpret. However, weighting of the data did not give as large an improvement as in a previous analysis of ToF-SIMS SIs [21]. The reason for this is that the dynamic range of EEL spectra is much less than that for ToF-SIMS. This means that the differences in error level between high and low spectral intensity is not large; correcting this by weighting the data will give only small improvements in the outcome.

In the analysis routines used in this paper, no restrictions were imposed on the sign of the components; they may be either positive or negative. Introducing the restriction of non-negativity [16] should lead to more readily interpretable loading spectra, but it may at the same time introduce some artefacts. Since part of the background-subtracted EEL spectra contains random noise around zero intensity, some of the data is, in reality, negative. As a result of the present approach, the loading spectra of the second- and higher-order components do not look like familiar EEL spectra. However, this is not necessarily a disadvantage for the analysis of ELNES. These components represent the *difference* from the average spectrum, which in many cases is an effective way to think about the manner in which the bonding is changing.

6. Conclusions

It has been shown that the principal component analysis of EEL spectrum images can be used to successfully extract and map compositional and bonding information. However, careful preprocessing of the EEL spectrum images is vital in order to remove experimental artefacts and obtain the best

results. Changes in spectral intensity due to changes in chemical composition or ELNES modulations can both be extracted as a single principal component. A shift in energy position of a spectral feature will lead to additional components, but the score images may still be used in an explorative manner. Areas of subtly changing spectra are highlighted, and can subsequently be used for further analysis.

The clear advantage of using PCA over conventional spectral processing methods is that it:

(1) can identify and locate spectral features such as ELNES modulations, that have not been anticipated by the operator; and
(2) can remove noise from the spectra without introducing additional artefacts or a loss in resolution.

Acknowledgements

Paul Thomas from the Software Group of Gatan Inc., UK, is kindly acknowledged for his Digital Micrograph script and advice on preprocessing EEL spectrum images. Paul Kotula from the Sandia labs., USA, is thanked for helpful discussions on MSA. This work was supported by the Australian Research Council.

References

[1] R.F. Egerton, Electron Energy-loss Spectroscopy in the Electron Microscope, second ed., Plenum Press, New York, 1996.
[2] V.J. Keast, A.J. Scott, R. Brydson, D.B. Williams, J. Bruley, J. Microsc. 203 (2001) 135.
[3] N.D. Browning, M.F. Chisholm, S.J. Pennycook, Nature 366 (1993) 143.
[4] P.E. Batson, Nature 366 (1993) 727.
[5] K. Suenaga, M. Tencé, C. Mory, C. Colliex, H. Kato, T. Okazaki, H. Shinohara, K. Hirahara, S. Bandow, S. Iijima, Science 290 (2000) 2280.
[6] M. Varela, S.D. Findlay, A.R. Lupini, H.M. Christen, A.Y. Borisevich, N. Dellby, O.L. Krivanek, P.D. Nellist, M.P. Oxley, L.J. Allen, S.J. Pennycook, Phys. Rev. Lett. 92 (2004) 095502-1.
[7] C. Jeanguillaume, C. Colliex, Ultramicroscopy 28 (1989) 252.
[8] J.A. Hunt, D.B. Williams, Ultramicroscopy 38 (1991) 47.
[9] E.R. Malinowski, Factor Analysis in Chemistry, third ed., Wiley, New York, 2002.
[10] A.F.H. Goetz, G. Vane, J.E. Solomon, B.N. Rock, Science 228 (1985) 1147.
[11] S. Beauchemin, D. Hesterberg, M. Beauchemin, Soil Sci. Soc. Am. J. 66 (2002) 83.
[12] K.M. Horn, B.S. Swartzentruber, G.C. Osbourn, A. Bouchard, J.W. Bartholomew, J. Appl. Phys. 84 (1998) 2487.
[13] P. Trebbia, N. Bonnet, Ultramicroscopy 34 (1990) 165.
[14] J.M. Titchmarsh, S. Dumbill, J. Microsc. 184 (1996) 195.
[15] J.M. Titchmarsh, Ultramicroscopy 78 (1999) 241.
[16] P.G. Kotula, M.R. Keenan, J.R. Michael, Microsc. Microanal. 9 (2003) 1.
[17] I.T. Jolliffe, Principal Component Analysis, second ed., Springer, New York, 2002.
[18] N. Bonnet, N. Brun, C. Colliex, Ultramicroscopy 77 (1999) 97.
[19] M. Meloun, J. Čapek, P. Mikšík, R.G. Brereton, Anal. Chem. Acta 423 (2000) 51.
[20] R. Bro, A.K. Smilde, J. Chemometr. 17 (2003) 16.
[21] M.R. Keenan, P.G. Kotula, Surf. Interface Anal. 36 (2004) 203.
[22] R.N. Cochran, F.H. Horne, Anal. Chem. 49 (1977) 846.
[23] G.Z. Chen, D.J. Fray, T.W. Farthing, Nature 407 (2000) 361.
[24] P.J. Thomas, Using the script 'ReplaceSpectrumInSIWithUI' Software Group, Gatan Inc., 2004.
[25] E. Anderson, Z. Bai, C. Bischof, S. Blackford, J. Demmel, J. Dongarra, J. Du Croz, A. Greenbaum, S. Hammarling, A. McKenney, D. Sorensen, LAPACK Users' Guide, third ed., Society for Industrial and Applied Mathematics, Philadelphia, PA, 1999. (Note: URL of the LAPACK web site: http://www.netlib.org/lapack, URL of the CLAPACK web site: http://www.netlib.org/clapack.)
[26] R.C. Whaley, A. Petitet, J.J. Dongarra, Parallel Comput. 27 (2001) 3 (Note: URL of the ATLAS web site: http://math-atlas.sourceforge.net/).
[27] M. Launay, F. Boucher, P. Moreau, Phys. Rev. B 69 (2004) 035101.